DØ note 4382-CONF

Measurement of Inclusive Jet and Dijet Cross Sections in $\bar{p}p$ collisions at $\sqrt{s} = 1.96\,\mathrm{TeV}$

The DØ Collaboration
URL: http://www-d0.fnal.gov

(Dated: March 25, 2004)

We present preliminary measurements of the inclusive jet and the dijet cross sections in $\bar{p}p$ collisions at a center-of-mass energy $\sqrt{s} = 1.96\,\mathrm{TeV}$. Jets are reconstructed using an iterative cone algorithm with radius $R_{\mathrm{cone}} = 0.7$. The data were acquired using the DØ detector during 2002 and 2003 and correspond to an integrated luminosity of $\mathrm{L} \simeq 140\,\mathrm{pb}^{-1}$. Results from next-to-leading order perturbative QCD calculations are compared to the cross section measurements.

Preliminary Results for Winter 2004 Conferences

Hadronic jet production with large transverse momentum (p_T) provides useful tests of perturbative QCD (pQCD) calculations. The inclusive jet and the dijet cross sections at large p_T or large invariant dijet mass ($M_{\rm jj}$) are directly sensitive to the strong coupling constant (α_s) and parton density functions (PDFs). Furthermore, potential deviations from the theoretical predictions at high p_T or $M_{\rm jj}$, not explained by PDFs or α_s, may indicate new physics beyond the Standard Model.

We present preliminary measurements of the inclusive jet and dijet cross sections at $\sqrt{s} = 1.96\,\text{TeV}$, based on a sample corresponding to an integrated luminosity of $\text{L} \simeq 140\,\text{pb}^{-1}$. Data were acquired with the upgraded DØ detector [1] in Run II of the Fermilab Tevatron. Events used in this analysis were triggered by single jet triggers, based on energy deposited in calorimeter towers. Data selection was based on run quality, event properties, and jet quality criteria.

Jets were defined by the "Run II cone algorithm" [2] which combines particles within a cone of radius $R_{\rm cone} = 0.7$ in rapidity, y, and azimuth, ϕ, around the cone axis. For data, calorimeter towers were combined into jets in the "E-scheme" (adding the four-vectors). This procedure was iterated until the solution stabilized. The four-vectors all towers were used as seeds in the first stage of the iterative procedure. The algorithm was re-run using the midpoints between pairs of jets as additional seeds (this makes the procedure infrared safe). Jets with overlapping cones were merged if the overlap area contained more than 50% of the p_T from the lower p_T jet, otherwise the particles in the overlap region were assigned to the nearest jet.

Data were corrected for the jet energy scale, selection efficiencies, and for migrations due to p_T or $M_{\rm jj}$ resolution. The jet energy scale was determined by minimizing the missing transverse energy in photon plus jet events. Spectra in p_T and $M_{\rm jj}$ were fit, in an iterative procedure, with parameterized ansatz functions and smeared with resolutions determined from data. Ratios of the original to the smeared ansatz functions were used to correct the data for migration effects. The highest p_T event in the data sample had $p_T = 616\,\text{GeV}/c$ and $M_{\rm jj} = 1206\,\text{GeV}/c^2$ and is displayed in Fig. 1 (see also Table I).

first jet	second jet
$p_T = 616\,\text{GeV}/c$	$p_T = 557\,\text{GeV}/c$
$y_{\rm jet} = -0.19$	$y_{\rm jet} = 0.25$
$\phi_{\rm jet} = 0.65$	$\phi_{\rm jet} = 3.78$
$M_{\rm jj} = 1206\,\text{GeV}/c^2$	

TABLE I: The quantities of the two leading jets in the event containing the highest jet p_T and invariant dijet mass, displayed in Fig. 1.

Both cross sections were measured in the central rapidity region, $|y_{\rm jet}| < 0.5$. The inclusive jet cross section is also presented for the forward region, $1.5 < |y_{\rm jet}| < 2.4$. The largest experimental uncertainty is due to the jet energy scale. Especially at highest p_T or $M_{\rm jj}$ (where the cross section is falling most steeply) these uncertainties become very large. Further contributions are from the efficiencies in the data selection, from trigger efficiencies, from uncertainties in the unsmearing procedure and from the determination of the jet p_T resolution. In addition, the luminosity measurement has an uncertainty of 6.5%.

Results are shown in Figs. 2 to 6. Fig. 2 shows the inclusive jet cross section as a function of p_T in three rapidity bins. Data are shown with statistical errors only. The jet cross section at large $y_{\rm jet}$ falls more steeply towards high p_T. The same distributions are displayed in Fig. 3, but with shaded bands indicating the systematic experimental uncertainties. These are dominated by the jet energy scale uncertainty. The dijet cross section is presented in Fig. 5.

Next-to-leading order (NLO) pQCD calculations are compared to the data in Figs. 2 to 6. The NLO calculations were computed using the program JETRAD [3]. The renormalization and factorization scales were set to half the leading jet p_T, $\mu_r = \mu_f = 0.5\,p_T^{\rm max}$. We used the CTEQ6M [4] parameterization of the PDFs and $\alpha_s(M_Z) = 0.118$. The maximum distance of particles within a jet was limited to $R_{\rm sep} \cdot R_{\rm cone}$ with $R_{\rm sep} = 1.3$ [5]. The ratio of data over theory is shown in Fig. 4. Uncertainties in the NLO calculations due to the PDF uncertainties are indicated by the grey bands; the experimental uncertainties are displayed as red lines. The latter increase with p_T, especially at large rapidities. Theory has good agreement with data given the large uncertainties.

We measured the inclusive jet and dijet cross sections in $\bar{p}p$ collisions at $\sqrt{s} = 1.96\,\text{TeV}$ based on a data sample corresponding to $\text{L} \simeq 140\,\text{pb}^{-1}$. The measurement of the dijet cross section was presented for $|y_{\rm jet}| < 0.5$ while the measurement of the inclusive jet cross section was extended to the larger rapidities. The data are well described by NLO pQCD throughout the whole kinematic region.

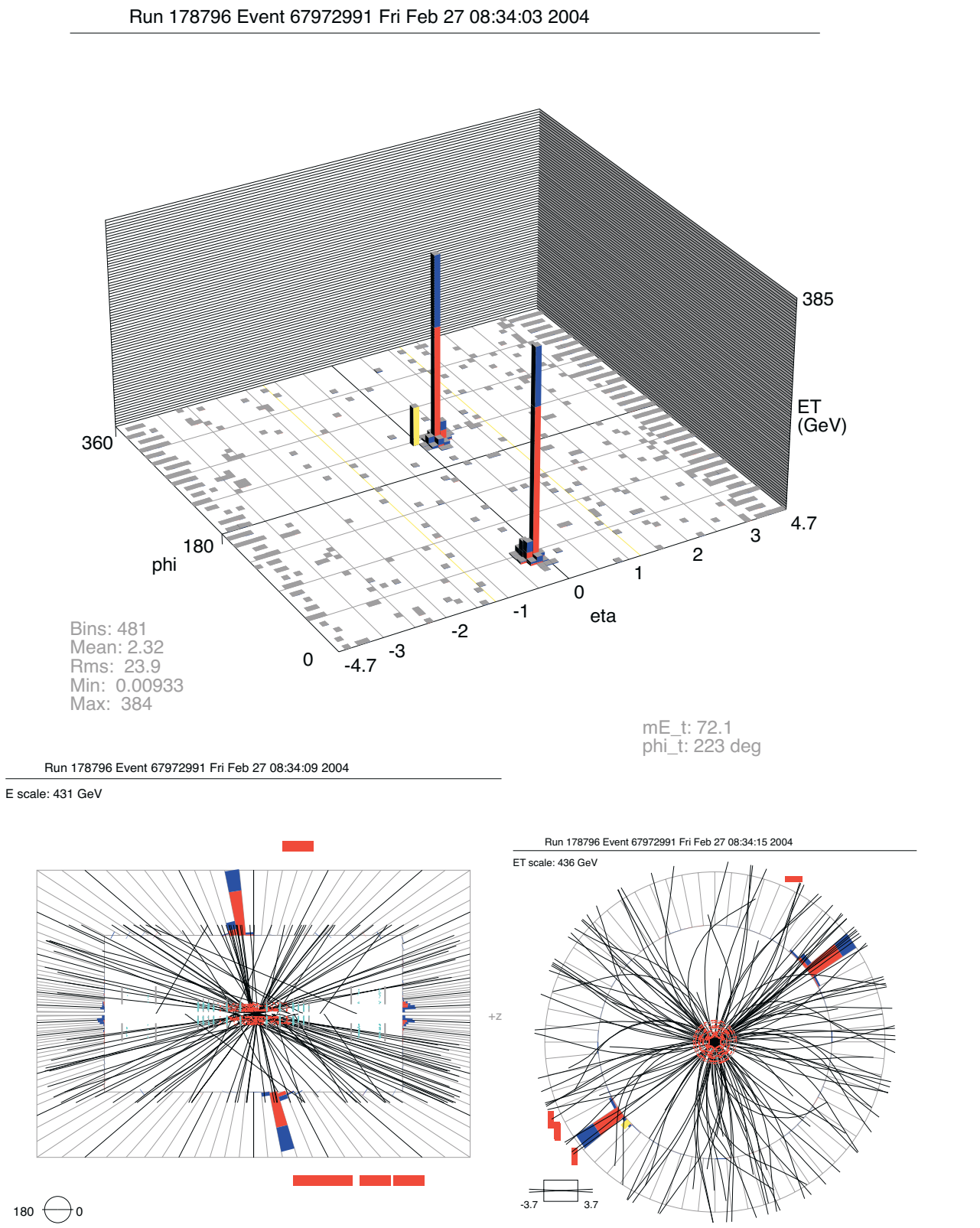

FIG. 1: Event 67972991 in Run 178796 had the highest observed invariant dijet mass ($M_{\rm jj} = 1206\,{\rm GeV}/c^2$) in the central rapidity region, $|y_{\rm jet}| < 0.5$. This is also the event with the highest jet p_T in the inclusive jet cross section measurement ($p_{T\,1} = 616\,{\rm GeV}/c$). Shown is the view in pseudorapidity and azimuth (top) and the RZ-view (bottom left) and the XY-view (bottom right).

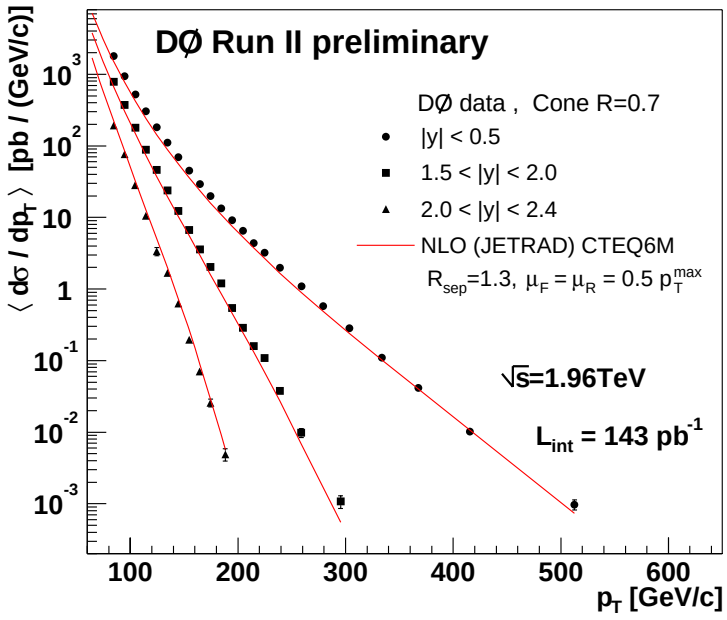

FIG. 2: The inclusive jet cross section, measured in different ranges of the jet rapidity (with statistical errors only). NLO pQCD calculations are overlayed on the data.

Acknowledgments

We thank the staffs at Fermilab and collaborating institutions, and acknowledge support from the Department of Energy and National Science Foundation (USA), Commissariat à L'Energie Atomique and CNRS/Institut National de Physique Nucléaire et de Physique des Particules (France), Ministry for Science and Technology and Ministry for Atomic Energy (Russia), CAPES, CNPq and FAPERJ (Brazil), Departments of Atomic Energy and Science and Education (India), Colciencias (Colombia), CONACyT (Mexico), Ministry of Education and KOSEF (Korea), CONICET and UBACyT (Argentina), The Foundation for Fundamental Research on Matter (The Netherlands), PPARC (United Kingdom), Ministry of Education (Czech Republic), Natural Sciences and Engineering Research Council and WestGrid Project (Canada), BMBF (Germany), A.P. Sloan Foundation, Civilian Research and Development Foundation, Research Corporation, Texas Advanced Research Program, and the Alexander von Humboldt Foundation.

[1] DØ Collaboration, F. Last, Nucl. Instrum. Methods A **123**, 456 (2004).
[2] Gerald C. Blazey et al.,"Run II Jet Physics", from "QCD and Weak Boson Physics in Run II", Fermilab-Pub-00/297, edited by U. Baur, R.K. Ellis, and D. Zeppenfeld, pp47-77 (2000).
[3] W.T. Giele, E.W.N. Glover, and D.A. Kosower, Phys. Rev. Lett. 73, 2019 (1994).
[4] J. Pumplin et al., JHEP 07, 12 (2002).
[5] S.D. Ellis, Z. Kunszt and D.E. Soper, Phys. Rev. Lett. 69, 3615 (1992).

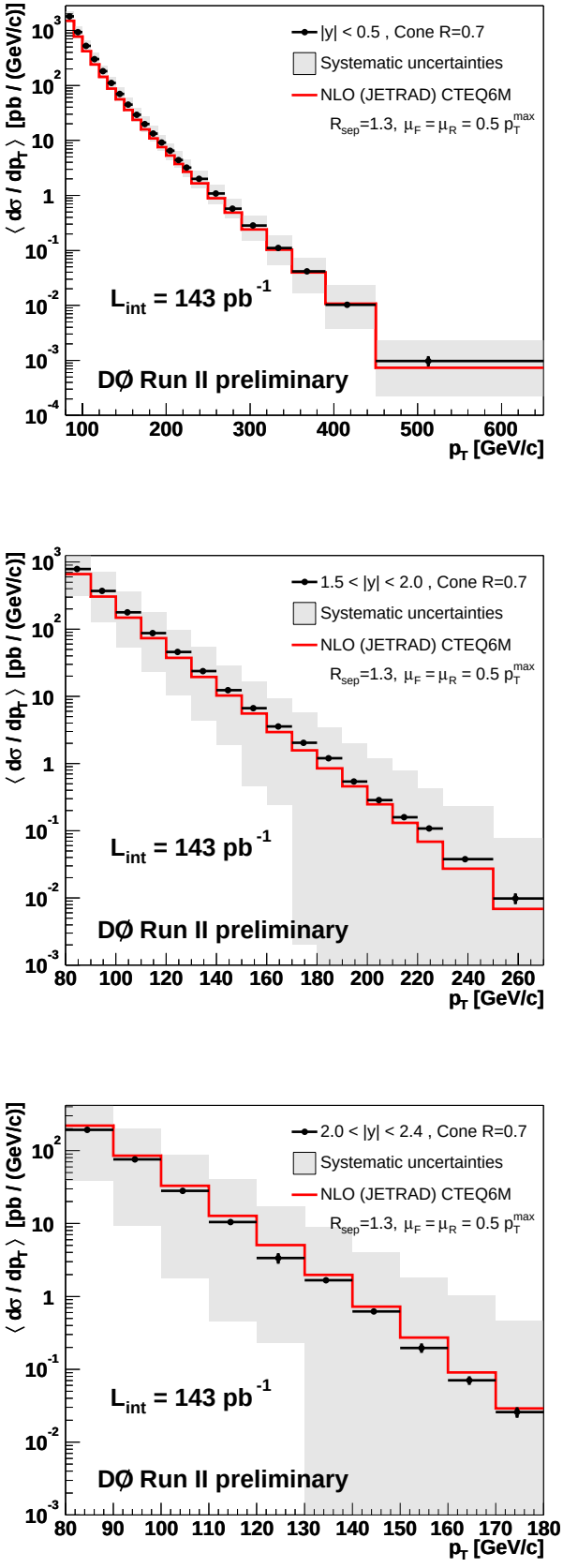

FIG. 3: The inclusive jet cross section, measured in different ranges of the jet rapidity. NLO pQCD calculations are overlayed on the data.

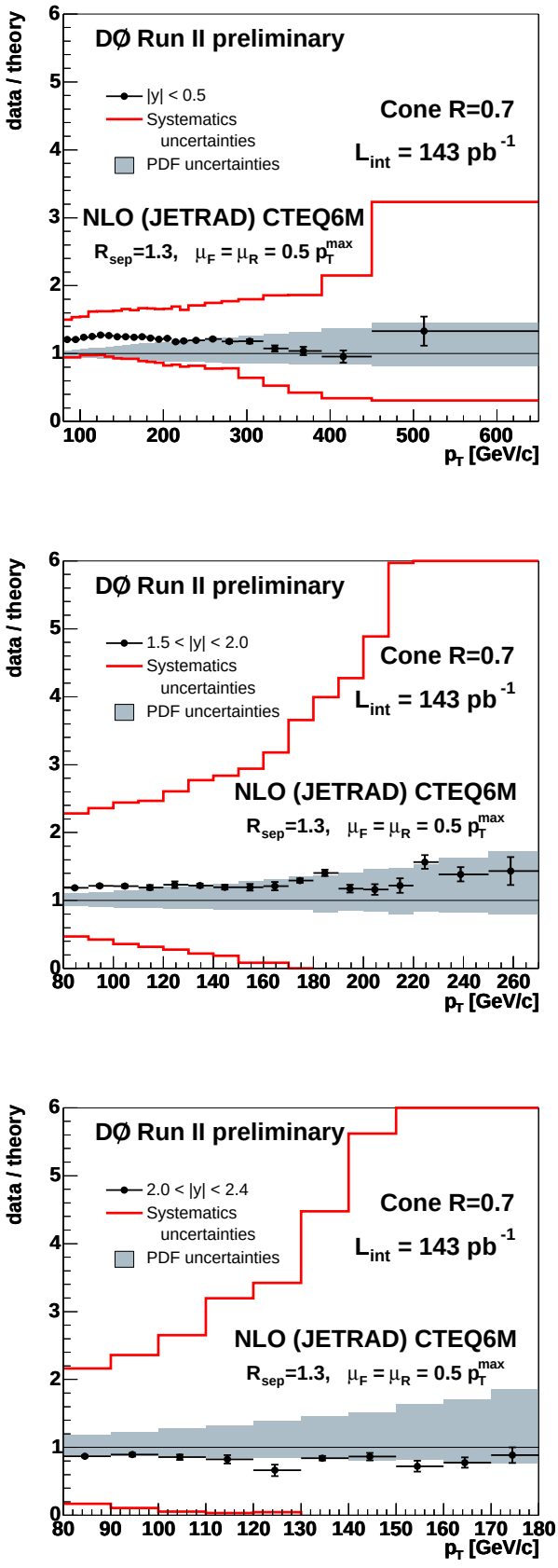

FIG. 4: The ratio of the measured inclusive jet cross section and the NLO pQCD calculations in three ranges of the jet rapidity. The experimental systematic uncertainties are displayed by the lines. The theoretical uncertainties due to the PDFs are shown as a grey band.

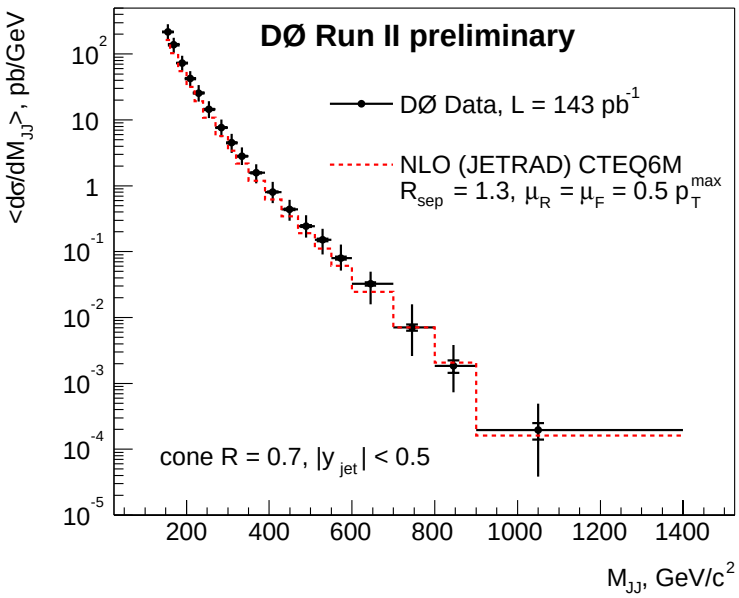

FIG. 5: The dijet cross section, measured at central rapidities. NLO pQCD calculations are overlaid on the data.

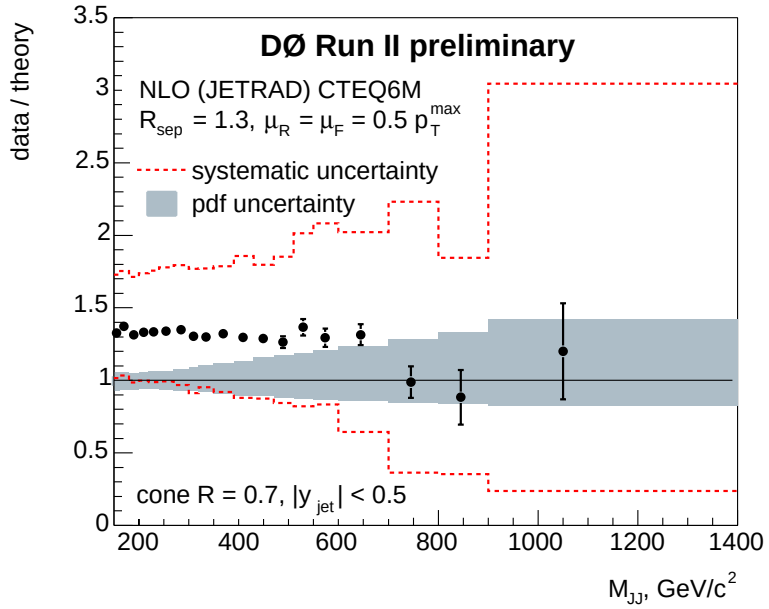

FIG. 6: The ratio of the measured dijet cross section, and the NLO pQCD calculations. The experimental systematic uncertainties are displayed by the dashed lines. The theoretical uncertainties due to the PDFs are shown as a grey band.